# A Novel Linear Precoder Design for Reliable UL/DL Detection in TDD Cellular Networks

Mohamed Salah Ibrahim, *Member, IEEE*, Ahmed Hussain, *Student Member, IEEE*, and Nicholas D. Sidiropoulos, *Fellow, IEEE* 

Abstract—The ever-growing demands on wireless connectivity, especially with the emergence of various data-intensive lowlatency applications, require novel multiplexing solutions capable of reliably supporting high rates at low latency. Non-orthogonal time division duplex (TDD) coupled with multiuser detection can meet these emerging needs, provided that accurate channel state information is available. This paper proposes a new pilot-free TDD frame structure that allows designing highly effective multiuser decoders and precoders for uplink and downlink multicell systems, in an unsupervised manner. The key idea is that each user repeats and permutes its uplink data using a pre-assigned permutation code. Invoking canonical correlation analysis (CCA) at the serving BS on the two deinterleaved uplink blocks yields high quality CCA-based beamformers capable of both recovering the uplink and precoding the downlink user signals in a way that effectively mitigates interference. The paper includes a pilotless synchronization framework that leverages CCA to recover the timing and frequency offsets in an asynchronous multiuser MIMO setup, without using pilots. Simulations are used to study the performance of the proposed approach on a largescale network with multiple users and cells, while laboratory experiments with a small-scale network of software radios are used to demonstrate that the approach works well in practice under common hardware imperfections.

Index Terms—Time division duplex (TDD), downlink, uplink, multiuser detection, multiple-input-multiple-output (MIMO), canonical correlation analysis (CCA), blind detection, repetition coding, identifiability, software defined radio (SDR), synchronization.

# I. INTRODUCTION

Supporting higher end-user data rates under the stringent requirements associated with the newly defined use cases in 5G/NR, namely ultra reliable low latency communication (URLLC) and enhanced mobile broadband (eMBB), represents a critical challenge for the next generation of cellular systems [1], [2]. The situation is further complicated by the emergence of new and diverse services, such as mobile virtual reality, and vehicle to everything (V2X) [3] services, which result in unprecedented strain on the available bandwidth [4].

Manuscript received April 3, 2022; revised August 24, 2022; accepted October 14, 2022. This work was supported by the National Science Foundation (NSF) under grants ECCS-2118002 and AST-2132700. The associate editor coordinating the review of this article and approving it for publication was M. Bennis. (Corresponding author: Mohamed Salah Ibrahim.)

Mohamed Salah Ibrahim was with the Department of Electrical and Computer Engineering, University of Virginia, Charlottesville, VA, 22904 USA (e-mail: salah@virginia.edu); he is now with InterDigital Communications, Conshohocken, PA 19428, USA.

Ahmed Hussain and Nicholas D. Sidiropoulos are with the Department of Electrical and Computer Engineering, University of Virginia, Charlottesville, VA, 22904 USA (e-mail: ahh6qxu,nikos@virginia.edu).

Such challenges have underscored the need to develop new technologies which are capable of providing higher system throughput and extremely low latency [5]. Multiple access is a key critical component of these technologies [6]. For instance, orthogonal multiple access techniques provide interference-free communication where different user transmissions happen in different time/frequency or use orthogonal codes, enabling the use of low complexity receivers. While orthogonal multiple access guarantees high end-user data rates as there is no interuser interference, this comes at the expense of latency due to the limited number of communication resources.

Spatial multiplexing and multiuser detection (MUD) enable simultaneous co-channel transmission and decoding of multiple user signals [7], [8], exploiting multiple antennas at the receiver to spatially separate the desired user signals. MUD techniques play a vital role in enhancing current communication systems performance [9]. MUD using maximum-likelihood (MLD) [7], the sphere decoder (SD) [10], or semi-definite relaxation (SDR) [11] can offer excellent detection performance but at very high computational complexity, thereby limiting the use of MUD in current cellular systems. Linear multiuser detectors, such as zero-forcing (ZF) and minimum mean square error (MMSE) [12], are more appropriate for adoption in practical systems [13] because of their lower complexity compared to MLD, SD, and SDR. Such a reduction in complexity, however, comes at the expense of performance, especially at low signal-to-noise ratios (SNR) and/or under near-far effects.

The common issue with all MUD techniques is that their performance is dependent on how accurate the channel estimates of the users are. In the context of cellular systems, the base station (BS) in each cell estimates the channels of the users that it serves using orthogonal pilot sequences transmitted by those users as well as users in neighbouring cells. The performance of channel estimation is also affected by the number of neighbouring cells considered in generating orthogonal pilot sequences — a problem referred to as pilot contamination [13], [14]. While estimating the served user channels allows ZF/MMSE based detectors/precoders to eliminate intra-cell interference, the inter-cell interference still remains and represents a major obstacle that impacts the performance of such methods.

This naturally raises the following question. Is it possible to bypass the channel estimation stage and directly design an *unsupervised*, *low-complexity* precoder capable of providing reliable communication in a multicell multiuser system?

In this paper we shall answer the above question in the

1

affirmative, by proposing a new pilot-free time division duplex (TDD) frame structure that involves a simple transmission strategy from the different users, which in turn allows the BS to efficiently design effective precoders for the users it serves. The key idea is that each user in the network forms two identical blocks of uplink data and then randomly interleaves the constructed blocks using a unique random permutation. By exploiting this line code structure, each multi-antenna BS first de-interleaves the received signal using the permutation associated with one of its assigned users. Then, the BS creates a pair of signal views that only share one common signal corresponding to the user whose permutation code was used – all other signals will still be randomly permuted since the permutation codes are unique. Applying canonical correlation analysis (CCA) to these two views, high-quality CCA-based precoders (also known as CCA canonical vectors) can be obtained to recover the uplink signal of the desired user even under strong inter- and intra-cell interference. The obtained CCA precoders are then used to beamform downlink user signals. More efficient TDD frame structures that can potentially improve the uplink data rates are also considered in this work.

CCA is a widely-used machine learning tool that aims at finding two linear combinations of two random vectors such that the resulting random variable is maximally correlated [15], [16]. Recently, we discovered a purely algebraic interpretation of CCA as a tool that identifies a shared "common" subspace between two signal views, under relatively mild conditions, even if the "uncommon" (not shared) components of each view are orders of magnitude stronger than the shared ones [17]. The application considered herein adds to the growing list of CCA applications including, but not limited to, equalization [18], radar [19], [20], blind source separation [21], [22], celledge user detection [17], [23], and multi-view learning [24], [25], to list a few.

Our contributions in this paper can be summarized as follows:

- We introduce a new pilotless TDD frame structure in a multicell multiuser network. The frame structure involves uplink packet repetition with interleaving followed by downlink data. Utilizing the uplink repetition together with the assigned unique UE permutation codes, each BS applies CCA multiple times to design high-quality precoders that can both recover the uplink signals in the phase of strong interference and be reused to beamform the downlink signals to the UEs served by the given BS.
- The proposed approach is entirely unsupervised in that it designs the different users precoders only by exploiting the repeated and interleaved uplink data. There is no need to estimate any user channel state information, and hence, it is by definition immune to channel estimation errors caused by near-far effects and pilot contamination. Further, the method works even if the user-transmitted signals are analog.
- Computationally, this paper shows that each BS is only required to perform two matrix inversions regardless of the number of users it serves; followed by one principal eigenvector computation (power iteration) for each user

- it serves. Hence, the proposed approach is attractive for practical implementation.
- The proposed approach can deal with practical communication system issues such as time and frequency synchronization. This paper proposes a lightweight algorithm that allows each BS to blindly identify the timing and carrier frequency offsets of the different users it serves, without using any pilots. Via exploiting the repetition structure, unique permutation codes and CCA, each BS performs a double-scan over time and frequency and tracks the resulting correlation coefficient of CCA. The method is shown to be effective in identifying the time and frequency offsets even for very weak users.
- Judicious simulations and laboratory experiments are carried out in order to convincingly demonstrate how well the proposed method works in practice. Simulations are first used to show the effectiveness of the proposed method in reliably recovering the uplink and downlink signals, assuming perfect channel reciprocity in a setup with seven hexagonal interfering cells. A realistic pathloss model from the 3GPP 38.901 specification is adopted to test the proposed method. Under different simulation settings, results show the superior performance of the pilot-free proposed method compared to ZF, MMSE and maximum ratio combining (MRC) baselines using fully orthogonal pilot sequences across all users in all cells thus incurring significant overhead and cell coordination, which our method does not use and does not need. In order to demonstrate the practical feasibility of our approach, we built and tested a prototype using software defined radios for a 2x2 MIMO network, where all the users are not synchronized. All users together with the multiple antenna BS were realized using USRP-2920 radios. We conducted multiple experiments including a scenario with near-far effects to assess the performance of the proposed CCA framework under realistic conditions. To maintain channel reciprocity, we used a well known algorithm to perform antenna calibration. Our laboratory experiments reveal that the proposed approach can, i) accurately estimate the timing and frequency offsets of the different users at the BS, ii) reliably recover the uplink user signals under power imbalance scenarios with order of magnitude lower BER compared to ZF, and iii) reliably decode the different users' downlink signals, despite imperfect reciprocity owing to the presence of

The remainder of this paper is organized as follows: Section II provides a brief review of CCA and its various formulations; Section III presents the system, signal, and channel model; Section IV introduces a new TDD frame structure and an uplink transmission protocol; Section V presents a proposed precoder design; Section VI proposes a new synchronization method to handle the asynchronous setup; Section VII provides numerical results including simulations and real experiments; and Section VIII draws conclusions.

small calibration errors.

#### II. CANONICAL CORRELATION ANALYSIS

Canonical correlation analysis (CCA) is a dimensionalityreducing technique that aims at finding linear relationships between two multi-dimensional data sets  $\mathbf{Y}_1 :=$  $[\mathbf{y}_{\ell}^{(1)},\cdots,\mathbf{y}_{\ell}^{(N)}] \in \mathbb{C}^{M_1 \times N}$  and  $\mathbf{Y}_2 := [\mathbf{y}_2^{(1)},\cdots,\mathbf{y}_{\ell}^{(N)}] \in \mathbb{C}^{M_2 \times N}$  using their second order statistics (cross-correlation and auto-correlation). Both data sets are assumed to be centered without loss of generality, otherwise their corresponding sample means are subtracted as a pre-processing step. Simply put, CCA seeks to find two base vectors  $\mathbf{q}_1 \in \mathbb{C}^{M_1}$  and  $\mathbf{q}_2 \in \mathbb{C}^{M_2}$ , known as canonical vectors, that aim at extracting two maximally correlated random variables from linear combinations of the entries of the random vectors  $y_1$  and  $y_2$ . From a mathematical point of view, the CCA problem can be expressed as [15], [16]

$$\begin{aligned} & \max_{\mathbf{q}_1, \mathbf{q}_2} & \operatorname{Re} \left\{ \mathbf{q}_1^H \mathbf{Y}_1 \mathbf{Y}_2^H \mathbf{q}_2 \right\} \\ & \text{s.t.} \quad & \mathbf{q}_{\ell}^H \mathbf{Y}_{\ell} \mathbf{Y}_{\ell}^H \mathbf{q}_{\ell} = 1, \quad \ell \in \left\{1, 2\right\}, \end{aligned} \tag{1b}$$

s.t. 
$$\mathbf{q}_{\ell}^{H} \mathbf{Y}_{\ell} \mathbf{Y}_{\ell}^{H} \mathbf{q}_{\ell} = 1, \quad \ell \in \{1, 2\},$$
 (1b)

where the two scaling constraints in (1) are used to avoid any trivial solutions. One appealing feature of CCA that makes it a favorable tool in practice is that solving the optimization problem (1) to find the canonical vectors  $\mathbf{q}_1$  and  $\mathbf{q}_2$  admits a simple algebraic solution via eigendecomposition [16]. Upon defining  $\Sigma_i = \frac{1}{N} \mathbf{Y}_i \mathbf{Y}_i^H$  as the sample auto-correlation of the random vector  $\mathbf{y}_i$  and  $\mathbf{\Sigma}_{ij} := \frac{1}{N} \mathbf{Y}_i \mathbf{Y}_j^H$  as the sample crosscorrelation of the two random vectors  $\mathbf{y}_i$  and  $\mathbf{y}_j$  for i, j = 1, 2and  $i \neq j$ , solving (1) is tantamount to solving the eigenvalue problem

$$\Sigma_{12}\Sigma_2^{-1}\Sigma_{21}\mathbf{q}_1 = \lambda\Sigma_1\mathbf{q}_1, \tag{2}$$

where it can be easily verified that the eigenvalue  $\lambda^*$  represents the square of the correlation coefficient,  $\rho$ , between the two vectors  $\mathbf{Y}_2^H \mathbf{q}_1$  and  $\mathbf{Y}_2^H \mathbf{q}_2$ , where  $\rho$  is defined as

$$\rho(\mathbf{q}_1^{\star}, \mathbf{q}_2^{\star}) = \operatorname{Re}\{\mathbf{q}_1^{\star H} \mathbf{Y}_1 \mathbf{Y}_2^H \mathbf{q}_2^{\star}\}. \tag{3}$$

Once the optimal  $\mathbf{q}_1^{\star}$  and  $\lambda^{\star}$  are obtained from solving (2), the optimal  $\mathbf{q}_2^{\star}$  can be obtained via direct substitution using

$$\mathbf{q}_2^* = \frac{1}{\sqrt{\lambda^*}} \mathbf{\Sigma}_2^{-1} \mathbf{\Sigma}_{21} \mathbf{q}_1^*. \tag{4}$$

An equivalent formulation of (1) is to minimize the Euclidean distance between the low-dimensional representations  ${\bf Y}_1^H {\bf q}_1$  and  ${\bf Y}_2^H {\bf q}_2$ . That is [16], [26]

$$\min_{\mathbf{q}_1, \mathbf{q}_2} \|\mathbf{Y}_1^H \mathbf{q}_1 - \mathbf{Y}_2^H \mathbf{q}_2\|_2^2$$
 (5a)

s.t. 
$$\mathbf{q}_{\ell}^{H} \mathbf{Y}_{\ell} \mathbf{Y}_{\ell}^{H} \mathbf{q}_{\ell} = 1, \quad \ell = 1, 2.$$
 (5b)

Expanding the cost of problem (5) and using the constraints, the equivalence between (1) and (5) can be easily verified; throughout this work, we will focus on the distance minimization formulation of CCA. Note that (1) and (5) can be naturally extended to find a multi-dimensional common subspace, e.g., see [17], but this is not needed herein, as we will only use single-component CCA.

In what follows, we will see how the canonical vectors in (5) can be used as high quality combiners/precoders that are capable of reliably decoding multiuser signals in TDD cellular networks, even under challenging scenarios, such as powerful interference or a severe near-far effects.

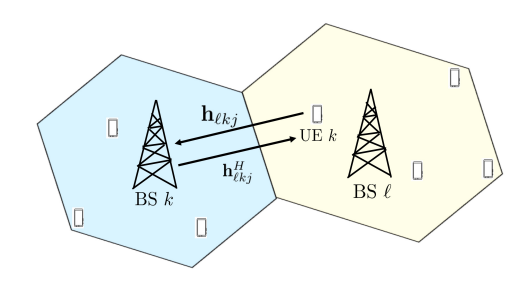


Fig. 1. System model.

#### III. SYSTEM AND SIGNAL MODELS

#### A. Channel Model

Consider a narrowband TDD cellular network comprising L cells, where each cell has radius R and is served by its own base station (BS), as shown in Fig. 1. The ℓ-th BS is equipped with  $M_{\ell}$  antennas, and serves  $K_{\ell}$  single-antenna user equipment (UE) devices, for  $\ell \in [L] := \{1, \dots, L\}$ . The uplink channel response from the k-th UE located in the  $\ell$ -th cell to the j-th BS is denoted by  $\mathbf{h}_{\ell k i} \in \mathbb{C}^{M_j}$ , and is modeled

$$\mathbf{h}_{\ell kj} = \sqrt{\beta_{\ell kj}} \mathbf{g}_{\ell kj},\tag{6}$$

where  $\mathbf{g}_{\ell kj} \in \mathbb{C}^{M_j}$  is the vector containing the small scale fading coefficients, while  $eta_{\ell kj} \in \mathbb{R}$  represents the large scale fading factor, for  $k \in [K_\ell] := \{1, \dots, K_\ell\}$  and  $\ell, j \in [L]$ . Note that for simplicity we assume that the large scale fading factor  $\beta_{\ell k j}$  describes the path-loss between the k-th UE located in the  $\ell$ -th cell and the j-th BS, and accordingly the users located in the j-th cell are served by the BS located in the same cell. Similarly, by exploiting the channel reciprocity feature of TDD systems, the downlink channel response between the BS in cell j and the k-th UE in cell  $\ell$  is denoted by  $\mathbf{h}_{\ell kj}^H$ , for  $\ell, j \in [L]$  and  $k \in [K_{\ell}]$ . The channel vectors of the users located in the j-th cell and the  $\ell$ -th BS can be expressed in a more compact form as

$$\mathbf{H}_{\ell j} = \mathbf{G}_{\ell j} \mathbf{D}_{\ell j}^{1/2},\tag{7}$$

where  $\mathbf{H}_{\ell j} = [\mathbf{h}_{\ell k j}, \cdots, \mathbf{h}_{\ell K_{\ell} j}] \in \mathbb{C}^{M_{j} \times K_{\ell}},$   $\mathbf{G}_{\ell j} = [\mathbf{g}_{\ell k j}, \cdots, \mathbf{g}_{\ell K_{\ell} j}] \in \mathbb{C}^{M_{j} \times K_{\ell}},$  and  $\mathbf{D}_{\ell j} = \mathrm{Diag}([\beta_{\ell k j}, \cdots, \beta_{\ell K_{\ell} j}]) \in \mathbb{R}^{K_{\ell} \times K_{\ell}}.$  Throughout this work, we assume that the channels are not known a priori, i.e. the receivers and transmitters have no knowledge of any channel state information in the network. Furthermore, we assume that the channels remain fixed within each coherence block (to be specified soon).

# B. Uplink and Downlink Signal Models

We assume that all cells are sharing the same frequency band. In other words, all UEs are transmitting their data over the same time-frequency physical resource block, i.e., nonorthogonal multiple access. For ease of exposition, we will begin with a synchronous setup where all user signals are synchronized at the BSs; however, our approach can effectively deal with the general asynchronous setup as we will see later. Towards this end, the discrete time baseband-equivalent model of the received multiantenna uplink (UL) signal at the  $\ell$ -th BS,  $\mathbf{Y}_{\ell} \in \mathbb{C}^{M_{\ell} \times T_u}$ , is given by

$$\mathbf{Y}_{\ell} = \sum_{k=1}^{K_{\ell}} \sqrt{p_{\ell k}} \mathbf{h}_{\ell k \ell} \mathbf{s}_{k \ell}^{T} + \sum_{j \neq \ell}^{L} \sum_{k=1}^{K_{j}} \sqrt{p_{j k}} \mathbf{h}_{j k \ell} \mathbf{s}_{k j}^{T} + \mathbf{W}_{\ell}, \quad (8)$$

where the first term in (8) represents the desired signals that need to be decoded at the  $\ell$ -th BS, while the second term refers to the interfering signal from the users in the neighbouring cells (inter-cell interference). The vector  $\mathbf{s}_{ki} \in \mathbb{C}^{T_u}$  refers to the uplink signal transmitted by the k-th user located in the i-th cell, where,  $T_u$  is the numebr of uplink symbols. Without loss of generality, we assume that  $\mathbb{E}[|\mathbf{s}_{ki}(n)|^2] = 1, \ k \in [K_i]$  and  $i \in [L]$ . Further, our approach does not impose any structure on the transmitted waveforms of the users, and different users can in fact have different waveforms (digital and/or analog). The term  $\mathbf{W}_\ell$  represents additive noise with independent and identically distributed (i.i.d) elements drawn from complex Gaussian distribution with zero mean and variance  $\sigma^2$ . Finally,  $p_{\ell k}$  represents the transmit power of the k-th UE in the  $\ell$ -th cell.

In this work, we assume that all UEs in all cells are active and are allocated the same power, i.e.  $p_{\ell k}=p_u, \ \forall k \in [K_\ell]$  and  $\ell \in [L]$ . In other words, power control and scheduling techniques are not considered in this work; however, they can be employed on top of the proposed method for service differentiation and additional performance improvements.

Given the received signal  $\mathbf{Y}_\ell$  at the  $\ell$ -th BS, our first objective is to unravel the uplink data for the users it serves, i.e.,  $\{\mathbf{s}_{k\ell}\}_{k=1}^{K_\ell}$ ,  $\forall \ell \in [L]$ . In order to separate the UEs' signals under strong inter- and intra-cell interference at their serving BS, the  $\ell$ -th BS needs to design receive beamformers  $\{\mathbf{q}_{k\ell} \in \mathbb{C}^{M_\ell}\}_{k=1}^{K_\ell}$  capable of recovering the signals of interest. Conventional beamforming solutions require accurate knowledge of the UEs' channel responses at their serving BS, i.e.,  $\mathbf{q}_{k\ell} = f(\hat{\mathbf{H}}_{\ell\ell})$ , where  $\hat{\mathbf{H}}_{\ell\ell}$  holds in its columns the estimated channel vectors of the served users.

In TDD systems, accurate channel estimation is done through sending uplink pilot sequences of length  $T_p$  at the beginning of the frame, as shown in Fig. 2(a), to obtain  $\hat{\mathbf{H}}_{\ell\ell}$ . The pilot sequence length  $T_p$  is a design parameter that needs to be carefully chosen to guarantee acceptable system performance. On one hand, long  $T_p$  affects the overall spectral efficiency, while short  $T_p$  degrades the UE channel estimates and makes the pilot contamination problem more severe. Even with perfect knowledge of the channel vectors for its own users, classical beamforming can still suffer from inter-cell interference, as the channels of users in other cells are much harder to estimate; only in-cell channels are estimated in practice.

Once the beamformers  $\{\mathbf{q}_{k\ell}\}_{k=1}^{K_\ell}$  are designed, the  $\ell$ -th BS estimates the k-th desired UE uplink signal as  $\mathbf{s}_{k\ell} = \mathbf{q}_{k\ell}^H \mathbf{Y}_\ell$ , for  $\ell \in [L]$ . Then, by exploiting the channel reciprocity feature of the TDD-based protocol [27], the BS transmits the downlink data to its desired UEs using  $\{\mathbf{q}_{k\ell}\}_{k=1}^{K_\ell}$  – this time as precoders (or, transmit beamformers). Following this

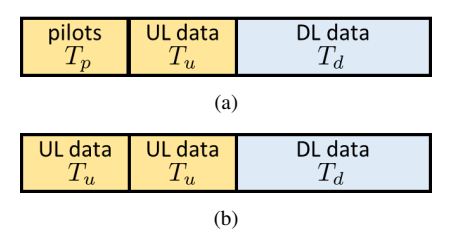


Fig. 2. (a) Traditional TDD frame structure. (b) Proposed TDD frame structure.

approach, the received DL signal,  $\mathbf{y}_{k\ell} \in \mathbb{C}^{1 \times T_d}$ , at the k-th UE served by the  $\ell$ -th BS can be expressed as

$$\mathbf{y}_{k\ell} = \mathbf{h}_{\ell k\ell}^{H} \sum_{k=1}^{K_{\ell}} \sqrt{\alpha_{k\ell}} \mathbf{q}_{k\ell} \mathbf{d}_{k\ell}^{T} + \sum_{j \neq \ell}^{L} \mathbf{h}_{jk\ell}^{H} \sum_{k=1}^{K_{j}} \sqrt{\alpha_{kj}} \mathbf{q}_{kj} \mathbf{d}_{kj}^{T} + \mathbf{w}_{k\ell}, \quad \forall k \in [K_{\ell}], \ell \in [L].$$

$$(9)$$

where  $\mathbf{d}_{k\ell} \in \mathbb{C}^{T_d}$  contains the DL payload data from the  $\ell$ -th BS to its k-th serving UE, and  $\alpha_{k\ell}$  stands for the corresponding allocated power to each UE. The term  $\mathbf{w}_{k\ell}$  represents noise with i.i.d entries drawn from a complex Gaussian distribution with zero mean and variance  $\sigma_d^2$ . Note that we take the DL channel as the Hermitian (conjugate) transpose of the UL channel, whereas reciprocity implies that the two are the same up to transposition. Our use of the Hermitian transpose is merely for mathematical and notational convenience. The classical uplink detection methods, namely zero-forcing (ZF) or minimum mean squared error (MMSE) (and their decisiondirected variants), require accurate channel estimates for the in-cell users to deliver acceptable detection performance. We will next propose a simple UE transmission protocol, which will be subsequently leveraged to obtain very effective UL/DL BS beamformers/precoders for use in multicell multiuser systems.

# IV. PROPOSED UPLINK TRANSMISSION SCHEME

Instead of using the traditional TDD frame structure that employs pilots, uplink data and then downlink data (see Fig. 2(a)), we propose a new frame structure that basically transmits the uplink data twice, followed by the downlink data. The uplink transmission scheme consists of two steps: repetition and interleaving. First, the k-th UE served by the  $\ell$ -th BS constructs two blocks by simply sending its signal  $\mathbf{s}_{k\ell} \in \mathbb{C}^{T_u}$  twice. Upon forming the two back-to-back blocks, i.e.,  $[\mathbf{s}_{k\ell}^T, \mathbf{s}_{k\ell}^T]^T$ , the k-th UE interleaves the  $2T_u$  symbols (samples for analog transmission), in a random manner. The transmitted signal,  $\mathbf{x}_{k\ell} \in \mathbb{C}^{2T_u}$ , from the k-th UE after repetition and interleaving can be written as

$$\mathbf{x}_{k\ell} = \mathbf{\Pi}_{k\ell} \begin{bmatrix} \mathbf{s}_{k\ell} \\ \mathbf{s}_{k\ell} \end{bmatrix}, \ \forall k \in [K_{\ell}], \ell \in [L].$$
 (10)

where  $\Pi_{k\ell} \in \mathbb{R}^{2T_u \times 2T_u}$  is a pseudo-random UE-specific permutation matrix. We assume that different UEs have different permutation matrices. Given that there are  $2T_u!$  possible permutation matrices, even with small  $T_u$ , e.g.,  $T_u = 32$ , there is a massive number of permutation matrices, making de-interleaving close to impossible unless the true permutation

matrix of the desired UE is known. Since the UE identities (IDs) are distinct and known at the serving BS, one can simply use them for generating different permutation matrices, that can be regenerated at the serving BS.

Upon plugging (6) in (8), the received signal at the  $\ell$ -th BS can be written in more compact form as

$$\mathbf{Y}_{\ell} = \sum_{i=1}^{L} \mathbf{H}_{\ell j} \mathbf{X}_{j}^{T} + \mathbf{W}_{\ell}, \quad \forall \ell \in [L].$$
 (11)

where  $\mathbf{X}_j := [\mathbf{x}_{kj}, \cdots, \mathbf{x}_{K_jj}] \in \mathbb{C}^{2T_u \times K_j}$  contains the UL transmitted sequences (after repetition and interleaving) of the UEs located in the j-th cell, and  $\mathbf{H}_{\ell j} \in \mathbb{C}^{M_j \times K_j}$  holds in its columns the respective channel vectors between the  $K_j$  users in cell j and BS  $\ell$ , as defined in (7). Also, for simplicity, the uplink transmit powers  $p_u$  have been absorbed in the corresponding channel vectors.

The goal now is to design  $\{q_{k\ell}\}_{k=1}^{K_\ell}$  beamformers at the  $\ell$ -th BS to be able to efficiently separate the associated UE signals, and then use such beamformers as precoders for downlink transmission. We will next present a novel UL beamformer / DL precoder design that is capable of both reliably decoding the uplink signals and effectively multiplexing the downlink signals of the UEs served by the  $\ell$ -th BS, even under strong inter- and intra-cell interference and without estimating any UE channel.

#### V. PROPOSED PRECODER DESIGN

Since the  $\ell$ -th BS knows its serving UE permutation matrices  $\{\Pi_{k\ell}\}_{k=1}^{K_\ell}$ , it can de-interleave its received signal  $\mathbf{Y}_\ell$  to obtain  $K_\ell$  matrices (one corresponding to applying the permutation matrix associated with each UE) as follows,

$$\mathbf{Y}_{k\ell} = \mathbf{Y}_{\ell} \mathbf{\Pi}_{k\ell}, \ \forall k \in [K_{\ell}]. \tag{12}$$

By exploiting the following property of permutation matrices

$$\mathbf{\Pi}_{k\ell}^T \mathbf{\Pi}_{ij} = \begin{cases} \mathbf{I}, & \text{if } k = i, \text{ and } \ell = j \\ \mathbf{\Pi}_{ki}^{(\ell j)}, & \text{otherwise} \end{cases}$$

where  $\Pi_{ki}^{(\ell j)}$  is another permutation matrix, one can see from (10) and (12) that the repetition structure will be only preserved for the k-th UE associated with the  $\ell$ -th cell while all the other UEs will be randomly permuted. Thus, (12) can be expressed as

$$\mathbf{Y}_{k\ell} = \mathbf{H}_{\ell\ell} \mathbf{S}_{\ell k\ell}^T + \sum_{j \neq \ell}^L \mathbf{H}_{\ell j} \mathbf{S}_{jk\ell}^T + \mathbf{V}_{k\ell}, \forall k \in [K_{\ell}]$$
 (13)

where  $V_{k\ell} := W_\ell \Pi_{k\ell}$  represents the resulting noise term after permutation. The matrices  $S_{\ell k\ell}$  and  $S_{jk\ell}$  contain the transmitted signals of the UEs associated with the  $\ell$ -th and j-th BSs, respectively, upon de-interleaving the signal received at the the  $\ell$ -th BS using the permutation code of the k-th UE assigned to the  $\ell$ -th BS. Matrix  $S_{\ell k\ell}$  can be expressed as

$$\mathbf{S}_{\ell k \ell} = \left[ \mathbf{\Pi}_{k \ell}^{T} \mathbf{\Pi}_{1 \ell} \begin{bmatrix} \mathbf{s}_{1 \ell} \\ \mathbf{s}_{1 \ell} \end{bmatrix}, \cdots, \begin{bmatrix} \mathbf{s}_{k \ell} \\ \mathbf{s}_{k \ell} \end{bmatrix}, \cdots, \mathbf{\Pi}_{k \ell}^{T} \mathbf{\Pi}_{K_{\ell} \ell} \begin{bmatrix} \mathbf{s}_{K_{\ell} \ell} \\ \mathbf{s}_{K_{\ell} \ell} \end{bmatrix} \right]$$

$$= \left[ \begin{bmatrix} \mathbf{s}_{1 \ell}^{(1)} \\ \mathbf{s}_{2}^{(2)} \end{bmatrix}, \cdots, \begin{bmatrix} \mathbf{s}_{k \ell} \\ \mathbf{s}_{k \ell} \end{bmatrix}, \cdots, \begin{bmatrix} \mathbf{s}_{K_{\ell} \ell}^{(1)} \\ \mathbf{s}_{K_{\ell} \ell} \end{bmatrix} \right]$$

$$(14)$$

where  $\mathbf{s}_{i\ell}^{(m)}$  represents the m-th resulting block of the i-th UE served by the  $\ell$ -th BS, for  $m=\{1,2\}$ . It is clear that the repetition structure is destroyed for all the UEs except for the k-th UE whose permutation matrix is used to obtain (14). Similarly, the matrix  $\mathbf{S}_{ik\ell}$  is defined as

$$\mathbf{S}_{jk\ell} = \left[ \mathbf{\Pi}_{k\ell}^T \mathbf{\Pi}_{1j} \begin{bmatrix} \mathbf{s}_{1j} \\ \mathbf{s}_{1j} \end{bmatrix}, \cdots, \mathbf{\Pi}_{k\ell}^T \mathbf{\Pi}_{K_j j} \begin{bmatrix} \mathbf{s}_{K_j j} \\ \mathbf{s}_{K_j j} \end{bmatrix} \right]$$
$$= \left[ \begin{bmatrix} \mathbf{s}_{1j}^{(1)} \\ \mathbf{s}_{2j}^{(2)} \\ \mathbf{s}_{1j}^{(2)} \end{bmatrix}, \cdots, \begin{bmatrix} \mathbf{s}_{K_j j}^{(1)} \\ \mathbf{s}_{K_j j}^{(2)} \end{bmatrix} \right]$$
(15)

where it can be easily seen that all the UEs associated with the j-th cell will be randomly permuted. By splitting the received signal in (13) into two blocks, one can construct the following two views

$$\mathbf{Y}_{k\ell}^{(1)} = \mathbf{H}_{\ell\ell} \mathbf{S}_{\ell k\ell}^{(1)T} + \sum_{j \neq \ell}^{L} \mathbf{H}_{\ell j} \mathbf{S}_{jk\ell}^{(1)T} + \mathbf{V}_{k\ell}^{(1)}, \qquad (16)$$

$$\mathbf{Y}_{k\ell}^{(2)} = \mathbf{H}_{\ell\ell} \mathbf{S}_{\ell k\ell}^{(2)T} + \sum_{j \neq \ell}^{L} \mathbf{H}_{\ell j} \mathbf{S}_{jk\ell}^{(2)T} + \mathbf{V}_{k\ell}^{(2)}.$$
 (17)

where the matrix  $\mathbf{S}_{\ell k \ell}^{(m)T}$  contains the data symbols in the m-th block of the matrix  $\mathbf{S}_{\ell k \ell}^{T}$ , i.e.,  $\mathbf{S}_{\ell k \ell}^{(m)T} = \mathbf{S}_{\ell k \ell}^{T}(1:T_u,:)$ , for  $m=\{1,2\},\ k\in[K_\ell]$  and  $\ell\in[L]$ . Note that the  $\ell$ -th BS has to construct  $K_\ell$  pairs of views; one pair for each serving UE. Given the constructed  $K_\ell$  pairs at the  $\ell$ -th BS, the goal is to design a set of combiners/precoders  $\{\mathbf{q}_{k\ell}\}_{k=1}^{K_\ell}$  to reliably decode the signals of interest of the UEs  $\{\mathbf{s}_{k\ell}\}_{k=1}^{K_\ell}$ .

Our design of the combiners/precoders is based on CCA. In a recent work [17], we have introduced a very useful new interpretation of CCA as a tool that can identify a common (shared) subspace between two matrix views, irrespective of how strong the non-shared components in each view are. Building upon this interpretation, and by looking at the two signal views in (16) and (17), one can see that the two matrices  $\mathbf{Y}_{k\ell}^{(1)}$  and  $\mathbf{Y}_{k\ell}^{(2)}$  share only one common component corresponding to the signal of the k-th UE of the  $\ell$ -th BS, whose permutation matrix was used to construct that pair. To show how the  $\ell$ -th BS can recover its k-th UE signal from  $\mathbf{Y}_{k\ell}^{(1)}$ and  $\mathbf{Y}_{k\ell}^{(2)}$ , we will use the so-called maximum variance (MAX-VAR) formulation of CCA [16]. Compared to the distance minimization formulation in (5), MAXVAR aims at finding a low dimensional common representation given two different data views. From an optimization perspective, the MAXVAR problem can be posed as

$$\min_{\mathbf{g}_{k\ell}, \mathbf{q}_{k\ell}^{(1)}, \mathbf{q}_{k\ell}^{(2)}} \sum_{j=1}^{2} \|\mathbf{Y}_{k\ell}^{T(j)} \mathbf{q}_{k\ell}^{(j)} - \mathbf{g}_{k\ell}\|_{2}^{2},$$
(18a)

$$\mathbf{s.t.} \quad \|\mathbf{g}_{k\ell}\|_2^2 = 1. \tag{18b}$$

where  $\mathbf{q}_{k\ell}^{(1)} \in \mathbb{C}^{M_\ell}$  and  $\mathbf{q}_{k\ell}^{(2)} \in \mathbb{C}^{M_\ell}$  are the two canonical vectors, and  $\mathbf{g}_{k\ell} \in \mathbb{C}^{T_u}$  is the resulting one-dimensional common subspace. In the two-views case, the above formulation is equivalent to the distance minimization (5) in the sense that both formulations yield the same optimal canonical vectors which can be obtained via solving for a principal eigenvector

as explained in Section II. In particular, the optimal solution of (18),  $\mathbf{q}_{k\ell}^{\star(1)}$ , is the principal eigenvector associated with the matrix  $\mathbf{A}_{k\ell} := \mathbf{\Sigma}_1^{-1(k\ell)} \mathbf{\Sigma}_{12}^{(k\ell)} \mathbf{\Sigma}_2^{-1(k\ell)} \mathbf{\Sigma}_{21}^{(k\ell)}$ , where  $\mathbf{\Sigma}_i^{(k\ell)} := \mathbf{Y}_{k\ell}^{(i)} \mathbf{Y}_{k\ell}^{T(i)}$  and  $\mathbf{\Sigma}_{ij}^{(k\ell)} := \mathbf{Y}_{k\ell}^{(i)} \mathbf{Y}_{k\ell}^{T(j)}$  are the autoand cross-correlation matrices, while  $\mathbf{q}_{k\ell}^{\star(2)}$  can be obtained using equation (4) with the appropriate auto- and cross-correlation matrices.

Define the matrix  $\mathbf{B}_{k\ell}^{(m)} = [\mathbf{S}_{1k\ell}^{(m)}, \cdots, \mathbf{S}_{\ell k\ell}^{(m)}, \cdots, \mathbf{S}_{Lk\ell}^{(m)}] \in \mathbb{C}^{T_u \times K_s}$ , and  $\mathbf{H}_{\ell} = [\mathbf{H}_{\ell\ell}, \mathbf{H}_{\ell j}] \in \mathbb{C}^{M_{\ell} \times K_s}$  with  $K_s := \sum_{\ell=1}^{L} K_{\ell}$ , for  $m \in \{1, 2\}, \ k \in [K_{\ell}]$ , and  $\ell \in [L]$ . We now have the following result.

**Theorem 1.** In the noiseless case, if the matrices  $\mathbf{B}_{k\ell}^{(m)} \in \mathbb{C}^{T_u \times K_s}$ , for  $\ell \in [L]$ , and  $\mathbf{H}_{\ell} \in \mathbb{C}^{M_{\ell} \times K_s}$  are full column rank, for  $j \in [L]$ , then the optimal solution  $\mathbf{g}_{k\ell}^{\star}$  of problem (18) is given by  $\mathbf{g}_{k\ell}^{\star} = \gamma_{k\ell} \mathbf{s}_{k\ell}$ , where  $\gamma_{k\ell} \in \mathbb{C}$ ,  $\gamma_{k\ell} \neq 0$  is a complex scaling factor.

*Proof.* The proof follows from Theorem 1 in [17].  $\Box$ 

Theorem 1 dictates that if the two full rank conditions are satisfied, then each BS can identify its serving UEs signals without knowing/estimating any UE channel, even for the weak UEs whose signals are overwhelmed by strong interand intra-cell interference. Satisfying the full rank condition though on the matrix  $\mathbf{B}_{k\ell}^{(m)}$  requires the packet length  $(T_u)$ to be greater than the total number of UEs in the network and the transmitted sequences to be linearly independent, for i = 1, 2. Both conditions can be easily satisfied with modest  $T_u$  since the different UE transmissions across all cells are independent. Further, to satisfy the full rank condition on the channel matrix H, we need the number of antennas at each BS to be greater than the total number of UEs in the system and the channel vectors of the different UEs to be linearly independent. The latter will be satisfied with probability one if the channel vectors are drawn from a jointly continuous distribution. Hence the most limiting assumption is that the total number of antennas at each BS is greater than or equal to the total number of users in the system. As we move towards massive MIMO and small-cell architectures in mmW frequencies, more BS antennas than active users is realistic. It is also worth noting that in practice we only need to account for the number of active interferers who are significantly above the noise floor at a given BS. We will show in simulations that even if  $M_{\ell}$  is only moderately greater than  $K_{\ell}$  but way less than  $K_s$ , our method still works well. In fact, the CCA beamformers will "automatically" eliminate the  $M_\ell - K_\ell$ dominant interferers and treat the others as noise. This is one striking observation of our experiments: that the strongest outof-cell interferers are automatically suppressed.

Note that in the noiseless case, the two resulting optimal canonical vectors obtained from solving (18) are identical (i.e.,  $\mathbf{q}_{k\ell}^{(1)} = \mathbf{q}_{k\ell}^{(2)}, \ \forall k \in [K_\ell]$  and  $\ell \in [L]$ , see proof of Theorem 1 in [17]. This arises from the fact that the channel vectors of the different users are the same across the two views. In the noisy case, however, the canonical vectors are generally different due to noise, and hence, for downlink transmission, the  $\ell$ -th BS constructs the k-th served UE precoder  $\mathbf{q}_{k\ell}$  by averaging

out the two resulting canonical vectors  $\mathbf{q}_{k\ell}^{(1)}$  and  $\mathbf{q}_{k\ell}^{(2)}$  followed by a pre-correction of the complex scaling factor  $\gamma$ , as follows

$$\mathbf{q}_{k\ell} = (\mathbf{q}_{k\ell}^{*(1)} + \mathbf{q}_{k\ell}^{*(2)})/2\gamma_{k\ell}, \forall k \in [K_{\ell}], \ell \in [L].$$
 (19)

where  $\mathbf{q}_{k\ell}^{*(1)}$  and  $\mathbf{q}_{k\ell}^{*(2)}$  are the conjugate of the optimal canonical vectors obtained from solving (18). The complex scaling factor,  $\gamma_{k\ell}$ , can be obtained by assuming that the first symbol is known at the receiver. While in the noiseless case or the high SNR regime, one pilot is enough to accurately estimate the phase, a few pilot symbols (e.g., four pilots) may be needed in the low SNR region. The precoder design procedure at the  $\ell$ -th BS is outlined in Algorithm 1. Once the

# Algorithm 1 CCA Precoder Design

 $\begin{array}{l} \text{Input: } \mathbf{Y}_{\ell} \in \mathbb{C}^{M_{\ell} \times 2T_{u}}, \\ \text{for } k = 1 : K_{\ell} \text{ do} \\ \mid \text{ Compute } \mathbf{Y}_{k\ell} := \mathbf{Y}_{\ell} \mathbf{\Pi}_{k\ell} \\ \mid \text{ Construct } \mathbf{Y}_{k\ell}^{(1)} := \mathbf{Y}_{k\ell} (:, 1 : T_{u}) \text{ and } \mathbf{Y}_{k\ell}^{(2)} := \mathbf{Y}_{k\ell} (:, T_{u} + 1 : 2T_{u}) \\ \mid \text{ Solve problem } (18) \text{ given } \mathbf{Y}_{k\ell}^{(1)} \text{ and } \mathbf{Y}_{k\ell}^{(2)} \\ \mid \text{ Obtain } \gamma_{k\ell} = \mathbf{g}_{k\ell}^{\star}(1)/\mathbf{s}_{k\ell}(1) \\ \mid \text{ Store } \mathbf{q}_{k\ell} = (\mathbf{q}_{k\ell}^{*(1)} + \mathbf{q}_{k\ell}^{*(2)})/2\gamma_{k\ell} \\ \text{end} \end{array}$ 

 $\ell$ -th BS obtains all  $K_{\ell}$  precoders (one for each UE it serves), it uses them for downlink transmission. Recall that the received downlink signal in (20) can be expressed in more compact form as,

$$\mathbf{y}_{k\ell} = \sum_{j=1}^{L} \mathbf{h}_{jk\ell}^{H} \mathbf{X}_j + \mathbf{w}_{k\ell}, \quad \forall k \in [K_{\ell}], \ell \in [L].$$
 (20)

where  $\mathbf{X}_j = \sum_{k=1}^{K_j} \mathbf{q}_{kj} \mathbf{d}_{kj}^T \in \mathbb{C}^{M_j \times T_d}$  is the transmitted signal from the  $\ell$ -th BS after applying its served UEs precoder. Towards this end, we have the following claim regarding the recovery of the downlink transmitted signals  $\{\mathbf{d}_{k\ell}\}_{k=1}^{K_\ell}, \forall \ell \in [L]$ .

**Theorem 2.** In the noiseless case, under the channel reciprocity assumption, the recovered downlink signal  $\mathbf{d}_{k\ell}$  upon applying the CCA precoder in (19), is given as  $\mathbf{d}_{k\ell} = \mathbf{y}_{k\ell}$ .

*Proof.* The proof is relegated to Appendix A.  $\Box$ 

# A. Computational Complexity

From Algorithm 1, the complexity of the proposed approach depends on the cost incurred in solving problem (18). The  $\ell$ -th BS needs to solve problem (18) for each of its assigned users. As explained in Section II, solving problem (18) requires solving an eigenvalue problem that involves two matrix inversions (of the auto-correlation matrices of the two signal views). Therefore, the  $\ell$ -th BS needs to perform  $2K_{\ell}$  matrix inversions to find the beamformers / precoders for the users it serves. The reason is that each BS first de-permutes the received signal using one of the permutation matrices of the UEs it serves, followed by separating the two back-to-back blocks to construct the two signal views, and hence, the two

auto-correlation matrices obtained for each UE are clearly different.

To reduce the computational complexity of the proposed approach, we propose a new design of the permutation matrices of the UEs that will later allow for performing only *two* matrix inversions per BS, irrespective of the number of users it serves. In particular, we have the following claim.

**Proposition 1.** Consider the model in (10), if the permutation matrix  $\Pi_{k\ell}$  is designed as

$$\mathbf{\Pi}_{k\ell} = \begin{bmatrix} \mathbf{\Pi}_{k\ell}^{(1)} & \mathbf{0} \\ \mathbf{0} & \mathbf{\Pi}_{k\ell}^{(2)} \end{bmatrix}, \tag{21}$$

then the two auto-correlation matrices of the two different constructed views for the k-th UE served by the  $\ell$ -th BS are the same for all UEs, where  $\Pi_{k\ell}^{(i)} \in \mathbb{R}^{T_u \times T_u}$ , for i = 1, 2,  $k \in [K_\ell]$  and  $\ell \in [L]$ .

# B. Uplink Transmission Rate Boosting

One of the main advantages of the proposed CCA approach relative to prior works that use CCA for common subspace estimation is that, owing to the design of the transmitted signals, the two views always share only one common signal (singledimensional common subspace). This significantly reduces the receiver complexity as opposed to the case with a multidimensional common subspace in our earlier work [17], [28], because the latter requires an additional stage to unravel the common signals form the resulting mixture, where depending on the adopted modulation and coding scheme, different methods can be employed to recover the original signals. Such methods are complex to implement in practice, especially for higher-order QAM signals (and do not work for analog amplitude-modulated signals). The one-dimensional common subspace provides a lot of flexibility on the structure of the transmitted waveform of all UEs. First, waveforms can all be analog across all UEs. Second, the proposed method can efficiently work and our recovery claim holds even if each UE is employing a different modulation scheme.

Perhaps one shortcoming of the proposed approach is that it requires repetition of the UE uplink data, thereby reducing the uplink transmission rate. However, it should also be noted that the proposed approach does not require the transmission of any training symbols (pilots), and hence, compared to legacy methods that use pilots for channel estimation, the number of uplink symbols can be set equal to the number of pilots, so attaining the same transmission rate of conventional multi-user detection schemes as we will see in Section VII. One possible approach that can improve the proposed method's transmission rate is that instead of repeating all uplink data  $(T_n)$  twice, one can repeat only a portion of the uplink data to design the beamformers that can be used to decode the rest of the uplink data (and subsequently reused for downlink precoding). For example, instead of using two blocks of the same data, each of length  $T_u$ , we can use two blocks with the same uplink data each of length  $(T_u/2)$  for finding the precoders followed by the remaining  $T_u$  uplink data. This pushes the uplink payload ratio to 0.75 from 0.5. Theoretically, in the absence of noise, our proposed approach can recover the common signals as long as the number of symbols per block (view) is greater than or equal to the number of UEs (see Theorem 1). In the presence of noise though, it has been shown [17] that increasing the number of symbols (samples) per view may improve the detection performance. This suggests that a careful choice of the size of each block (view) can potentially improve the transmission rate without considerably hurting the detection performance.

# VI. BLIND CFO AND TIMING ESTIMATION

One major challenge that we encounter in real multiuser communication systems is the timing and carrier frequency offset (CFO) estimation of the co-channel users at their serving BS. While there are indeed powerful solutions that can deal with synchronization issues, such methods primarily rely on using training symbols to find the time and frequency offsets (e.g., using cross-correlation), and for near-far power imbalance scenarios, long training sequences are required for the weak UEs to accurately estimate the timing offset. In this section, we propose a novel and fully blind synchronization method that can find the timing and frequency offsets of the different UEs at their serving BS even in aggressive power imbalance scenarios. This makes the end-to-end approach fully blind without any need for transmitting pilots for channel estimation or CFO and timing acquisition.

Instead of transmitting long and orthogonal pilot sequences to find the start time of the different UEs signals at the BS, we propose a practical CCA-based synchronization framework that leverages the repetition structure of the uplink signals of the UEs to accurately acquire the timing and CFO of the different UEs. The main idea is to scan the received signal at the BS across time and frequency, where at each instant the BS uses the permutation codes of a given UE to construct two signal views, applies CCA on these two views, and measures the resulting correlation coefficient. The correlation coefficient will peak whenever we hit the right timing and CFO for that UE.

In practical systems, the  $\ell$ -th BS receives a long sequence,  $\overline{\mathbf{Y}}_{\ell} \in \mathbb{R}^{M_{\ell} \times \overline{T}}$  where  $\overline{T} > 2T_u$  represents the number of samples collected at the UE before synchronization. Given the uplink received signal at the  $\ell$ -th BS, the goal is to find the timing offset,  $m_{k\ell}$  and the CFO  $\omega_{k\ell}$  associated with the k-th UE served by the  $\ell$ -th BS,  $\forall k \in [K_{\ell}]$  and  $\ell \in [L]$ . To do so, we first define a CFO window with boundaries  $w_{\min}$  and  $w_{\max}$ , discretized to  $N_w$  points. To find the correct CFO and timing for the k-th UE, the  $\ell$ -th BS iterates over the  $N_w$  different frequency points,  $\{w_n\}_{n=1}^{N_w}$ , and for each  $w_n$ , the BS corrects for the CFO via element-wise multiplying each row of its received signal,  $\overline{\mathbf{Y}_{\ell}}$  by the vector  $\mathbf{v}_n^T$ , where

$$\mathbf{v}_n = [1, \exp(j2\pi w_n), \cdots, \exp(j2\pi w_n(\overline{T} - 1))]^T. \quad (22)$$

Once the CFO is corrected using  $w_n$ , the  $\ell$ -th BS performs a time scan over M points. Starting with m=1, the  $\ell$ -th BS first constructs the signal  $\overline{\mathbf{Y}}^{(m)} = \overline{\mathbf{Y}}(:, m: 2T_u + m - 1)$  (note the BS index is dropped for ease of notation). Second, the BS

re-permutes the signal  $\overline{\mathbf{Y}}^{(m)}$  to obtain  $\mathbf{Y}^{(mk)}$  using its k-th UE permutation code. Finally, the BS separates the two blocks  $\overline{\mathbf{Y}}_1^{(mk)} = \overline{\mathbf{Y}}^{(m)}(:,1:T_u)$  and  $\mathbf{Y}_2^{(mk)} = \overline{\mathbf{Y}}^{(m)}(:,T_u+1:2T_u)$  followed by applying CCA on the two resulting views and storing the correlation coefficient  $\rho_{mn}$ , where  $m \in [M] := \{1,\cdots,M\}$  and  $n \in [N_w] := \{1,\cdots,N_w\}$ .

The BS repeats the above procedure at all timing and CFO points. If we hit the correct CFO  $w_{nk}^{\star}$  and the start point  $m^{\star}$  of the two back-to-back blocks of the k-th UE, then the resulting correlation coefficient from CCA of the two separated block "views" will attain its peak. In other words, after iterating over time and frequency, CCA should yield  $K_{\ell}$  distinct peaks associated with the  $K_{\ell}$  UEs served by the  $\ell$ -th BS. The power of the peak will depend on the received SNR of the respective UEs as we will see in the experiments. It is worth pointing that the proposed blind synchronization method only utilizes the repetition structure of the UE uplink signals together with the CCA-based receiver to find the timing and CFO of the different UEs, and it has nothing to do with the waveform used at each UE (it can even work for analog transmissions). The procedure is summarized below in Algorithm 2.

# Algorithm 2 CCA-based Timing and CFO Estimation

Note that each BS needs to run Algorithm 2, possibly in parallel, for a total of  $K_\ell$  times. The complexity of Algorithm 2 is dominated by solving problem (18). As explained in Section II, solving (18) is tantamount to solving a maximum eigenvalue problem of a matrix whose computation involves two matrix inversions. The maximum eigenvector can be cheaply computed using the power method. It is worthemphasizing that, for the proposed synchronization method to work properly, we need the received signal power to be a few dBs above the noise floor (e.g., SNR = 5 dB). In the case of the very low SNR, pilot based synchronization may be used as a fallback option if needed.

To further reduce the complexity of Algorithm 2, one can use the permutation matrix design proposed in Section V to compute the two matrix inversions once for all UEs per each

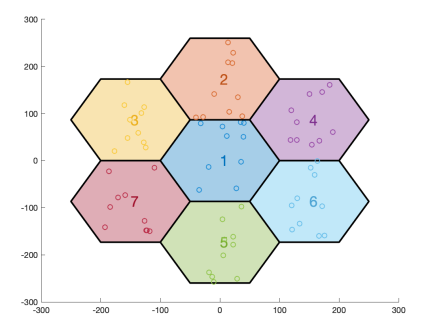


Fig. 3. Snapshot of the simulated scenario with seven cells.

time index and CFO index. Further, instead of computing the two matrix inversions each time index, i.e., for each m, one can exploit the fact that any increment in m results in removing the first sample and appending one more sample to the constructed signal at time m, i.e.,  $\overline{\mathbf{Y}}^{(m+1)}$  is the same as  $\overline{\mathbf{Y}}^{(m)}$  except for one sample. Thus, the auto-correlation matrices obtained at time m+1 are merely two rank-one updates of the auto-correlation matrices obtained at time m, and hence, one can use the Sherman-Morrison formula to find the inversions of the auto-correlation matrices in closed form at time m,  $\forall m \in \{2, \cdots, M\}$ .

# VII. NUMERICAL RESULTS

In this section, we we will first use numerical simulation to assess the performance of the proposed method in multiuser multicell scenarios with a large number of users. Then, we will demonstrate that our approach works well in practice through real experiments using software defined radios (SDRs). In the hardware experiments, we will consider a 2x2 MIMO setup comprising two non synchronized UEs communicating with a two-antenna BS.

# A. Simulation Results

Throughout this subsection, we will use a simulated scenario with L=7 hexagonal cells, each of radius R=100 meters and a BS located at its center, as shown in Fig. 3. The number of antennas at the  $\ell$ -th BS was set to  $M_\ell=M=16$  antennas, and the number of users assigned to the  $\ell$ -th BS was set to  $K_\ell=10$  UE devices, unless stated otherwise.

Each BS is serving only the UEs located in its cell (see the color codes in Fig. 3). The UEs locations are chosen uniformly at random up to distance R from the center of each cell. The downlink packet length was set to  $T_d = 1024$  while the uplink packet length was set to  $T_u = 256$ . The transmit power of all users was set to  $p_{\ell k} = 20$  dBm  $\forall k \in [K_\ell]$  and  $\ell \in [L]$ . In the downlink, the  $\ell$ -th BS transmit power was set to 35 dBm divided equally across its served UEs, and the noise power was set to  $\sigma^2 = -80$  dBm. We used 500 different user drops, each with 200 different Monte Carlo trials. Within each Monte Carlo trial, the uplink transmit signals  $\mathbf{s}_{k\ell}$ , downlink transmit signals  $\mathbf{d}_{k\ell}$ , uplink noise matrix  $\mathbf{W}_{\ell}$ , downlink noise vectors  $\mathbf{w}_{k\ell}$ , and channel matrices  $\mathbf{H}_{\ell j}$  (except for the drop-dependent path losses) are all drawn randomly,  $\forall k \in [K_{\ell}], \ \ell \in [L]$ .

<sup>&</sup>lt;sup>1</sup>We use MATLAB notation, i.e.,  $\mathbf{X}^{(k)} = \mathbf{X}(:, k: N+k-1)$  contains all the rows of matrix  $\mathbf{X}$  and a subset of columns of  $\mathbf{X}$  starting from the k-th column and ending with the (N+k-1)-th column.

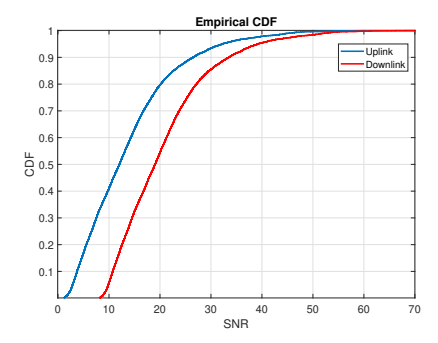


Fig. 4. The CDF of the average received SNR.

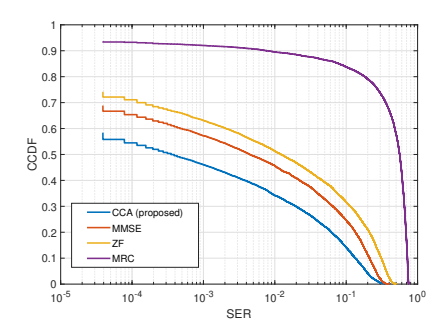


Fig. 5. Uplink SER CCDF with  $M_\ell=16$  and  $K_\ell=10$ .

The uplink channel between the  $\ell$ -th BS and the k-th user in the j-th cell is modeled as

$$\mathbf{h}_{\ell kj}^{H} = \sqrt{\frac{1}{M}} \sum_{n=1}^{N_p} \sqrt{\beta_{\ell kj}^{(n)}} \mathbf{g}_{\ell kj}^{H}$$
 (23)

where  $N_p$  is the number of paths between the  $\ell$ -th BS and the k-th user in cell  $j, \ \forall \{\ell,j\} \in [L]$  and  $k \in [K_\ell]$ , and is randomly chosen between [5,15]. The path gain,  $\beta_{\ell k j}^{(n)}$ , is computed using the path-loss model of the urban macro (UMa) scenario from Table 7.4.1-1 in the 3GPP 38.901 standard, with the carrier frequency set to  $f_c=2$  GHz. Further, all UEs in all cells are allowed to possibly have a line of sight (LOS) component to their serving BS according to the LOS probability expression for the UMa scenario in Table 7.4.2-1 in the 3GPP 38.901 standard. The vector  $\mathbf{g}_{\ell k j}$  represents the small scale fading coefficients with its elements drawn from a complex circularly symmetric Gaussian distribution with zero mean and unit variance.

For the proposed CCA based detector, we use the proposed frame structure in Fig. 2(b), where the uplink data is repeated twice. At each BS, we separate the two uplink blocks and use CCA on the two constructed signal views to find the CCA-based beamformers/precoders. We use four pilots to resolve the (complex) scaling ambiguity that is inherent in CCA. Note that the scaling ambiguity is corrected after recovering the common signal using CCA. Also, to further improve the uplink detection performance, when detecting the uplink signals, we average out the resulting signals from  $\mathbf{Y}_{k\ell}^{T(1)}\mathbf{q}_{k\ell}^{(1)}$  and  $\mathbf{Y}_{k\ell}^{T(2)}\mathbf{q}_{k\ell}^{(2)}$  prior to scaling correction and hard detection.

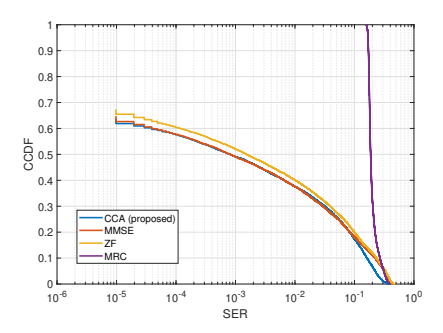


Fig. 6. Downlink SER CCDF with  $M_{\ell}=16$  and  $K_{\ell}=10$ .

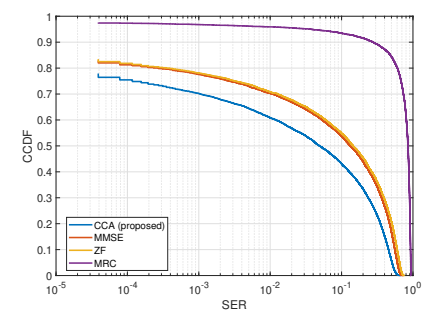


Fig. 7. Uplink SER CCDF, 16PSK,  $M_{\ell}$  = 32,  $K_{\ell}$  = 10.

To assess the efficacy of our approach, we use the following approaches as performance baselines, i) **ZF** / **MMSE**: The channels of all users associated with a given BS are estimated at their serving BSs with the help of orthogonal pilot sequences (across all UEs in all cells, no pilot contamination) of length  $T_p = 256$  transmitted by each UE. This way, the total redundancy is kept the same, with baselines using 256 symbols as pilots followed by 256 as UL payload, and our method transmitting the same payload of length 256 twice. Then, the MMSE or ZF detector is employed to decode the UE signals using their estimated channels, and ii) **MRC**: The maximum ratio combining detector using the same UE channel estimates.

In the first simulation, we considered QPSK modulation for all UEs in all cells. To measure the uplink and downlink performance, we report the complementary cumulative distribution function (CCDF) of the symbol error rate (SER) across all UEs in all cells. We simulated 500 different UE drops where in each drop we have 10 UEs per cell.

Before reporting the SER performance, we observe from the uplink received SNR distribution (blue curve in Fig. 4) that the uplink average received SNR is less than 4.5 dB for 15% of the UEs, more than 22.5 dB for 15% of the UEs and between 4.5 dB and 22.5 dB for 70% of the UEs the SNR. Now by looking at the CCDF of the SER in Fig. 5, we observe that the proposed CCA approach made no detection errors in our (extensive) simulation for 42% of the UEs, while the corresponding percentages for MMSE and ZF are 32% and 25%, respectively. This corresponds to UEs with at least 14 dB, 16 dB and 18.5 dB for CCA, MMSE and ZF, respectively, which means that CCA provides 2 dB SNR gain over MMSE. Furthermore, Fig. 5 shows that CCA achieves more than an

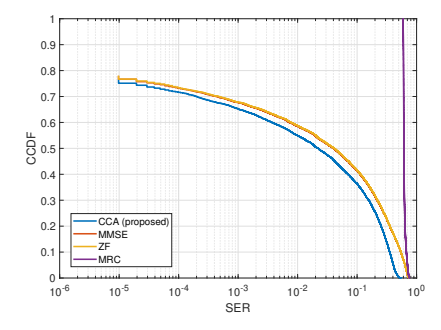


Fig. 8. Downlink SER CCDF, 16PSK,  $M_{\ell}$  = 32,  $K_{\ell}$  = 10

order of magnitude reduction in the average SER  $(3\times10^{-4})$  at 50% compared to MMSE  $(4\times10^{-3})$  and ZF ( $10^{-2}$ ). Finally, CCA achieves 0.1 SER for roughly 85% of the UEs (minimum 4.5 dB SNR) relative to 75% of the UEs (minimum 6.7 dB SNR) and 65% of the UEs (minimum 8.7 dB SNR) for MMSE and ZF, respectively. This demonstrates the effectiveness of the proposed CCA approach in the low SNR region where it can achieve 2.2 dB SNR gain relative to MMSE.

For the downlink performance, one can see from Fig. 6 that CCA attains the same SER approximately achieved by MMSE (only slight improvement for CCA at the high SNR region where CCA and MMSE made no errors for 61% and 64%, respectively).

Next, we simulated another scenario where all UEs are employing 16PSK modulation and the number of transmit antennas at the BS is set to 32. All other parameters are kept the same, and hence, we have the same SNR distribution in Fig. 4. Fig. 7 shows that the uplink performance degraded with all the CCDF curves compared to Fig. 5 are shifted as expected. One can see that with 16PSK modulation, CCA achieves on average (50-percentile of the CCDF) 0.04 SER compared to 0.13 SER makes no errors for 22% of the UEs as opposed to 16% for MMSE and ZF. This corresponds to UEs with average SNR greater than 19.5 dB for CCA and 21 dB for both MMSE and ZF. In downlink, CCA outperforms both MMSE and ZF by achieving 0.02 SER for 50% relative to 0.04 for ZF and MMSE as Fig. 8 depicts.

In the previous simulations, the uplink packet length  $T_p$ was set to 256 symbols and was repeated one time as shown in Fig. 2(b). To further improve the uplink transmission rate, instead of repeating the entire uplink packet and thus having two blocks of size  $T_u$  each, we shrink the size of the repeated blocks to be of size  $T'_u$  each and use these blocks to construct the CCA precoders which will be used to detect the rest of the uplink packet and then used for the downlink. In this case, the uplink payload data will be  $2T_u - T'_u$  as opposed to only  $T_u$ . We evaluated the uplink performance with  $T'_u$ set to  $0.4T_u$ ,  $0.6T_u$ ,  $0.8T_u$  and  $T_u$ , where  $T_u = 250$ . Low  $T'_{u}$  values yield higher uplink rate but at the same time degrade the CCA performance. Fig. 9 shows the CCDF of the SER achieved by our proposed method for the different values of  $T'_u$ . With  $T'_u = T_u$ , one can see that CCA achieves the best SER (blue curve), outperforming the MMSE with  $T_p = T_u$  (which operates at the same UL transmission rate)

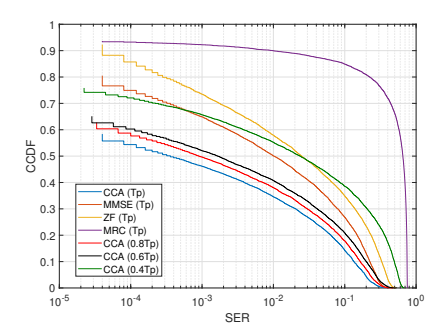


Fig. 9. Uplink SER CCDF with different repetition size,  $T_p$  = 256 symbols.

by more than an order of magnitude improvement in SER. More interestingly, with  $T_u^\prime=0.6T_u$  (black curve), CCA still significantly outperforms the MMSE in terms of SER and also achieves better uplink rate with uplink payload size equal to 350 symbols compared to 250 symbols for the MMSE. This suggests that with a slight sacrifice in the performance, CCA can significantly improve the uplink transmission rate.

#### B. Experimental Results

In this subsection, we performed real-world tests of the proposed method in various experimental setups.

1) Hardware Setup: we used multiple National Instruments USRP-2920 software-defined radios (SDRs) to demonstrate practical implementations of the proposed framework. To do so, we built a 2x2 prototype using SDRs. BS and UEs are built using USRP-2920 devices linked to general-purpose computers as shown in Fig. 10. The USRPs are used for radio signal transmission / reception, while the computers are used for baseband signal processing. For the purpose of time and frequency synchronization of the antenna downconversion chains at the BS, a 10 MHz eight-port reference clock from a CDA-2990 external clock module with GPS Disciplined Oscillator (GPSDO) was used. The clock is connected with a GPS antenna which is used for driving the pulse per second (PPS) signals to the clock. The UEs are located in different locations, and hence, they are not synchronized. The experiments were conducted in an indoor static environment with two single-antenna UEs, each realized using a standalone USRP-2920. The BS, however, has three synchronized single-antenna USRPs (one is used for calibration purposes for maintaining reciprocity) as shown in Fig. 11(a). The two UEs have line-of-sight link with the BS as shown in Fig. 10. The locations of UEs and the BS are fixed throughout the experiments. The distances between the UE1, UE2 and the BS are 5, and 3.5 meters, respectively. The transmit power of the UEs is set to 5 dBm, unless stated otherwise, while the transmit power of the BS is set to 20 dBm. The sampling rate used in the experiments is set to 1 mega samples per second (MS/sec), the signal bandwidth is 100 KHz, and the carrier frequency is 1.2 GHz.

2) Uplink and Downlink Processing: In the uplink, each UE transmits two identical back-to-back blocks of QPSK symbols of length 128 symbols per block, then the symbols



Fig. 10. Experimental setup.

(a) (b) (c)

Fig. 11. (a) Base station. (b) UE1. (c) UE2.

are shuffled using a unique random generator for each UE. The random generator IDs are known at the BS. The constructed signals are then oversampled by a factor of 10, then the resulting oversampled signal is passed through a square-root raised cosine (SRRC) pulse shaper with roll-off factor and amplitude set to 0.5 and 6, respectively. The pulse shaped signal is zero-padded with a number of zeros equal to one third of the packet, yielding a sequence of length 4020 samples. This results in a transmission rate of 64 Kbps for all UEs. The zero-padding is also used at the receiver side to measure the received SNR, as we will see later. Symbol generation, upsampling, and pulse shaping are all done in MATLAB. Then, the transmit data of each user is fed to GNU radio before being wirelessly transmitted.

At the receiver side, the BS performs matched-filtering with the same filter used at the UEs. Then, the BS uses the proposed synchronization method in Algorithm 2 to estimate the timing and CFO of each UE. Once the synchronization parameters are found, the BS uses them to correct the CFO and then identify the start of the two back-to-back blocks of each UE, deinterleave with the associated code, separate the two blocks and then pass the two views to CCA. For the considered baselines (ZF and MRC), we still use our synchronization method to find the synchronized UE packets. Then, we estimate the channel vector for each UE using one of the blocks symbols as pilots, then we use the estimated channel vector for each UE to decode the UEs packet using ZF and MRC.

In the downlink, we use the Argos calibration method proposed in [29] to maintain channel reciprocity. Such a method requires using a reference antenna at the BS to perform the calibration (that is why we always use one more antenna at the BS as we will see later). The BS constructs the CCA beamformer by averaging out the two resulting canonical

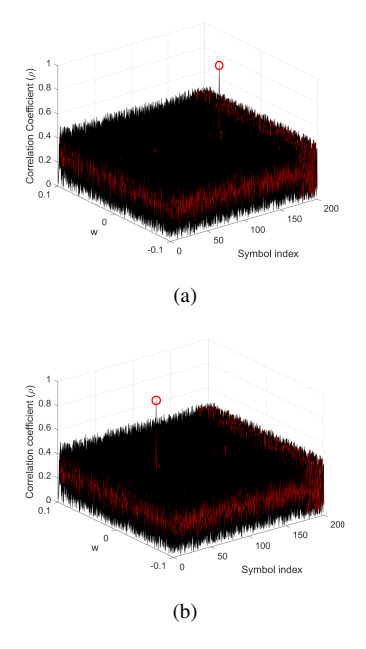


Fig. 12. Timing and CFO recovery using Algorithm 2 for (a) UE1. (b) UE2.

vectors for each UE followed by correcting the inherent phase ambiguity. Then the BS splits its available power budget across the UEs, precodes and adds the downlink signals of the UEs followed by using the same pulse shaper used in the uplink. At the receiver, the UE merely performs temporal matched filtering followed by a phase correction assuming 10 pilots out of the 256 transmitted symbols.

# C. Performance Evaluation.

The considered 2x2 setup involved the use of two UEs (noted as UE1 and UE2 in Fig 10) and a BS with 3 active USRPs; out of these 3 radios, 2 were used for uplink and downlink communication while the third one was used as a reference antenna for Argos calibration [29]. All USRPs are equipped with a single vertically-oriented antenna.

To show how well our proposed CCA-based synchronization method works, we tested the proposed method in both the 2x2 and 3x3 MIMO setups. For each setup, we ran Algorithm 2 with  $N_w$  set to 500, the CFO window boundaries  $w_{\rm min}$  and  $w_{\rm max}$  set to  $-10^{-2}$  and  $10^{-2}$ , respectively, and the number of time points set to M=200. The 3D plots in Fig. 12 demonstrate how effective the proposed synchronization approach is in recovering the timing and CFO of the UEs. One can clearly see a distinct peak corresponding to the right timing and CFO of UE1 and UE2 in Fig. 12(a) and Fig. 12(b), respectively.

To show the efficacy of our proposed method in practice, we start with a balanced setup where the two UEs transmit at the same power, 10 dBm. The measured received SNR of each UE at the BS in this case is approximately 22.5 dB, and all methods (CCA, ZF and MRC) make no errors that we could record in this case. Fig. 13 shows the scatter plots of the soft received symbols of both UEs in uplink and downlink using our proposed CCA method. Fig. 13(a) and 13(b) depict how well-clustered the received symbols from the two UEs are prior

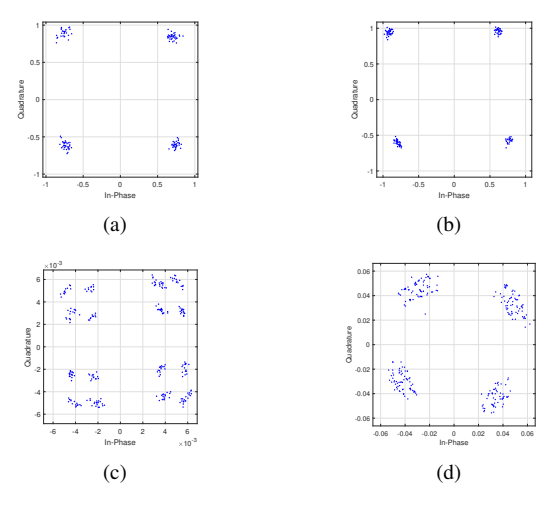


Fig. 13. The scatterplots of the received symbols of the two UEs in uplink and downlink. a) UE1 in uplink. b) UE2 in uplink. c) UE1 in downlink. d) UE2 in downlink

to detection using the proposed method, while Fig. 13(c) and 13(d) demonstrate the effectiveness of the CCA precoders in spatially isolating the downlink signals of the two UEs. While the received symbols in the downlink are clearly separated in the four quadrants, they are not well-clustered as in the uplink. We attribute this to imperfect channel reciprocity, which only holds approximately even when (imprefect) Argos calibration is used. Still, the results are very satisfactory, confirming that reciprocity is a reasonable assumption.

Next, we set up a power imbalanced scenario where we reduce the power of UE2 to be -5 dBm while UE1 is kept at 10 dBm. To visualize the power imbalance between the two UEs, the two plots in Fig. 14(a) and Fig. 14(b) show the received packets of both UEs at one of the two antennas after synchronization and matched filtering but before downsampling. Looking at the received samples energy of UE2 in Fig. 14(b), one can clearly see two signal levels: the higher level at -20 dB corresponds to the strong user (UE1) signal covering the weak user (UE2) one and the other (-35 dB) corresponding to part of UE2 signal overlapping with the padded zeros of UE1. Further, after downsampling, we plot the energy of the 256 received symbols at one of the two antennas for the two UEs, Fig. 14(c) shows that the symbol energy is centered around -20 dB for all symbols while for UE2 one can obviously see the fluctuations of the power due to the existence of the two power levels as depicted in 14(d). This shows how UE2 is overwhelmed by UE1.

We now compare the resulting SER for both UEs in uplink and downlink. We observed that all methods make no symbol errors in the uplink for UE1 (strong user). For UE2, however, one can see from Fig. 15(a) that the proposed method achieves less than  $10^{-3}$  SER which is an order of magnitude less that ZF which attains 0.04 SER. Further, MRC completely fails due to the large power imbalance between the two UEs. In the downlink, Fig. 15(b) reveals the superiority of CCA where UE1 and UE2 achieve 0.006 and 0.015 SER, respectively.

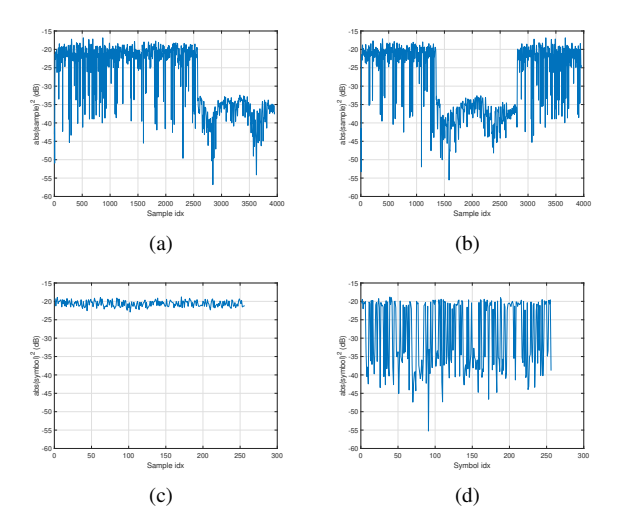


Fig. 14. Snapshot of the received packets of UE1 and UE2. a) Sample energy UE1. b) Sample energy UE2. c) Symbol energy UE1. d) Symbol energy UE2

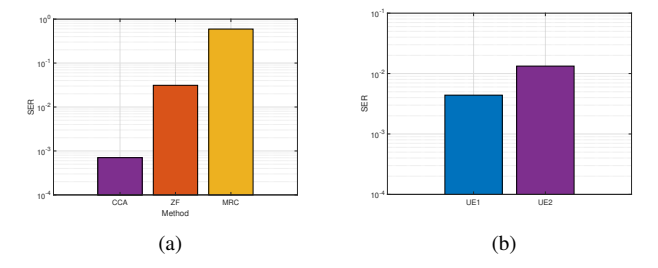


Fig. 15. SER performance of a 2x2 setup. a) Uplink results for UE2. There were no errors recorded for UE1. b) Downlink results of UE1 and UE2 using CCA.

# VIII. CONCLUSIONS

In this paper, we proposed a new pilot-free TDD frame structure that involves uplink data repetition followed by downlink data. The proposed frame structure requires each UE to repeat its uplink data followed by randomly permuting the two uplink blocks via a unique pre-determined permutation code (e.g., based on the UE equippment ID). Constructing two signal views after de-permuting using one of the UE codes, a receive beamformer for that UE can be obtained using CCA. We showed that the CCA-derived beamformer is theoretically guaranteed to recover the uplink signal of that UE, under high inter-cell and intra-cell interference; and it reliably does so in practice. Further, we verified that, with perfect channel reciprocity, downlink user signals can be accurately precoded to "isolate" the downlink transmissions in a way that theoretically allows simple interference-free downlink decoding at the UE. We then proposed a novel pilotfree synchronization framework that can accurately estimate timing and carrier frequency offsets for each UE, in an asynchronous multiuser MIMO setup, without using any pilots. We demonstrated through simulations on a large scale multiuser multicell MIMO network that the proposed method achieves striking performance compared to existing methods that rely on orthogonal pilot transmission to accurately estimate the

UE channels. To further validate how practically feasible the proposed approach is, we tested the proposed method and synchronization framework in a real world wireless testbed, where experiments using software defined radios revealed the superiority of the proposed method in an asynchronous setup involving two UEs and a two-antenna BS.

# APPENDIX A PROOF OF THEOREM 2

The proof utilizes the optimal CCA canonical vectors obtained from the proof of Theorem 1. Given the signals  $\mathbf{Y}_{k\ell}^{(1)}$  and  $\mathbf{Y}_{k\ell}^{(2)}$  in (16) and (17), respectively, it follows from the proof of Theorem 1 that, the optimal canonical vectors are given as

$$\mathbf{q}_{k\ell}^{(j)} = \gamma_{k\ell} \mathbf{H}_{\ell}^* (\mathbf{H}_{\ell}^T \mathbf{H}_{\ell}^*)^{-1} \mathbf{e}_{k\ell}$$
 (24)

where j=1,2 and  $\gamma_{k\ell}\in\mathbb{C}$  is a complex scaling ambiguity. The vector  $\mathbf{e}_{k\ell}\in\mathbb{R}^{K_s}$  has one at the location of the signal of interest and zero otherwise. The scaling ambiguity of the different UEs  $\{\gamma_{k\ell}\}_{k=1}^{K_\ell}$  served by the  $\ell$ -th BS can be easily resolved via correlation with each UE identification sequence. Now, let us construct the k-th UE precoder as

$$\mathbf{q}_{k\ell} = (\mathbf{q}_{k\ell}^{*(1)} + \mathbf{q}_{k\ell}^{*(2)})/2\gamma_{k\ell}$$

$$= \mathbf{H}_{\ell}(\mathbf{H}_{\ell}^{H}\mathbf{H}_{\ell})^{-1}\mathbf{e}_{k\ell}$$
(25)

By stacking all the precoders  $\mathbf{q}_{k\ell}$  designed at the  $\ell$ -th BS, for  $k \in [K_\ell]$  and  $\ell \in [L]$ , in a matrix  $\mathbf{Q}_\ell \in \mathbb{C}^{M_\ell \times K_\ell}$ ,  $\forall \ell \in [L]$ , the noise-free received signal at the k-th UE served by the  $\ell$ -th BS can be expressed as,

$$\mathbf{y}_{k\ell} = \sum_{j=1}^{L} \mathbf{h}_{jk\ell}^{H} \mathbf{Q}_{j} \mathbf{D}_{j}^{T} \quad \forall k \in [K_{j}], j \in [L].$$
 (26)

where  $\mathbf{D}_j := [\mathbf{d}_{1j}, \cdots, \mathbf{d}_{K_j j}] \in \mathbb{C}^{T_d \times K_j}$ . We can write (26) in more compact form as,

$$\mathbf{y}_{k\ell} = \mathbf{h}_{k\ell}^H \mathbf{Q} \mathbf{D}^T \quad \forall k \in [K_s], \ell \in [L]. \tag{27}$$

where  $\mathbf{h}_{k\ell} = [\mathbf{h}_{1k\ell}^T, \cdots, \mathbf{h}_{Lk\ell}^T]^T \in \mathbb{C}^{M_s}$ , and  $M_s = \sum_{\ell=1}^L M_\ell$ . Further, the matrices  $\mathbf{D} \in \mathbb{C}^{T_d \times K_s}$  and  $\mathbf{Q} \in \mathbb{C}^{M_s \times K_s}$  are defined as  $\mathbf{D} := [\mathbf{D}_1, \cdots, \mathbf{D}_L]$  and

$$\mathbf{Q} = egin{bmatrix} \mathbf{Q}_1 & & & \ & \mathbf{Q}_2 & & \ & & \mathbf{Q}_L \end{bmatrix},$$

respectively. It can now be readily verified that  $\mathbf{h}_{k\ell}^H \mathbf{Q}$  is equal to a row vector with one at the location of the signal of interest and zero otherwise, thus  $\mathbf{y}_{k\ell} = \mathbf{d}_{k\ell}$ .

# APPENDIX B PROOF OF PROPOSITION 1

Let us write the permutation matrix  $\Pi_{k\ell}$  introduced in (10) as

$$\mathbf{\Pi}_{k\ell} = \begin{bmatrix} \mathbf{\Pi}_{k\ell}^{(1)} & \mathbf{0} \\ \mathbf{0} & \mathbf{\Pi}_{k\ell}^{(2)} \end{bmatrix}$$
 (28)

where  $\Pi_{k\ell}^{(i)} \in \mathbb{R}^{T_u \times T_u}$ , for  $i=1,2,\ k \in [K_\ell]$  and  $\ell \in [L]$ . Exploiting the block diagonal structure of the permutation matrix used for each UE, it can be easily seen that randomly permuting each block separately allows the  $\ell$ -th BS to first separate the received signal to two blocks and then use the two random codes  $\Pi_{k\ell}^{(1)}$  and  $\Pi_{k\ell}^{(2)}$  of the k-th UE to align the corresponding signal views. This block partitioning of the permutation matrices ensures that the auto-correlation matrices of the two views will be the same for all UEs associated with a given BS. To see this, let us split the received signal  $\mathbf{Y}_\ell$  into two parts  $\mathbf{Y}_\ell^{(1)}$  and  $\mathbf{Y}_\ell^{(2)}$ , i.e.,  $\mathbf{Y}_\ell = [\mathbf{Y}_\ell^{(1)}, \mathbf{Y}_\ell^{(2)}]$ . Then, using  $\mathbf{Y}_\ell$  and the permutation matrix in (21), (12) can be expressed as

$$\mathbf{Y}_{k\ell} = [\mathbf{Y}_{\ell}^{(1)}, \mathbf{Y}_{\ell}^{(2)}] \begin{bmatrix} \mathbf{\Pi}_{k\ell}^{(1)} & \mathbf{0} \\ \mathbf{0} & \mathbf{\Pi}_{k\ell}^{(2)} \end{bmatrix}, \ \forall k \in [K_{\ell}].$$
 (29)

Now, by constructing the two views associated with the k-th UE served by the  $\ell$ -th BS, it follows that

$$\mathbf{Y}_{k\ell}^{(1)} = \mathbf{Y}_{\ell}^{(1)} \boldsymbol{\Pi}_{k\ell}^{(1)}, \ \mathbf{Y}_{k\ell}^{(2)} = \mathbf{Y}_{\ell}^{(2)} \boldsymbol{\Pi}_{k\ell}^{(2)}.$$

By computing the auto-correlation matrices of the two views, one can obtain  $\Sigma_{k\ell}^{(j)} = \frac{1}{T_u} \mathbf{Y}_{k\ell}^{(j)} \mathbf{Y}_{k\ell}^{(j)H}$ , for j=1,2. Using the fact that  $\Pi_{k\ell}^{(j)} \Pi_{k\ell}^{(j)} = \mathbf{I} \ \forall k,\ell$ , then it can be readily seen that  $\Sigma_{k\ell}^{(j)} = \mathbf{Y}_{\ell}^{(j)} \mathbf{Y}_{\ell}^{(j)H} = \Sigma_{\ell}^{(j)}$ . This shows that the auto-correlation matrices are the same across all UEs served by BS  $\ell$ , hence, only two matrix inversions are required at each BS to design the CCA based beamformers / precoders.

# REFERENCES

- [1] E. Dahlman, G. Mildh, S. Parkvall, J. Peisa, J. Sachs, Y. Selén, and J. Sköld, "5G wireless access: requirements and realization," *IEEE Communications Magazine*, vol. 52, no. 12, pp. 42–47, 2014.
- [2] W. Saad, M. Bennis, and M. Chen, "A vision of 6G wireless systems: Applications, trends, technologies, and open research problems," *IEEE Network*, vol. 34, no. 3, pp. 134–142, 2019.
  [3] S. Chen, J. Hu, Y. Shi, Y. Peng, J. Fang, R. Zhao, and L. Zhao,
- [3] S. Chen, J. Hu, Y. Shi, Y. Peng, J. Fang, R. Zhao, and L. Zhao, "Vehicle-to-everything (V2X) services supported by LTE-based systems and 5G," *IEEE Communications Standards Magazine*, vol. 1, no. 2, pp. 70–76, 2017.
- [4] H. Ullah, N. G. Nair, A. Moore, C. Nugent, P. Muschamp, and M. Cuevas, "5G communication: an overview of vehicle-to-everything, drones, and healthcare use-cases," *IEEE Access*, vol. 7, pp. 37 251–37 268, 2019.
- vol. 7, pp. 37 251–37 268, 2019.

  [5] N. Al-Falahy and O. Y. Alani, "Technologies for 5G networks: Challenges and opportunities," *IT Professional*, vol. 19, no. 1, pp. 12–20, 2017.
- [6] J. Boccuzzi, "Introduction to cellular mobile communications," in Multiple Access Techniques for 5G Wireless Networks and Beyond, 2019, pp. 3–37.
- [7] S. Verdu et al., Multiuser detection. Cambridge University Press, 1998.
- [8] D. Tse and P. Viswanath, *Fundamentals of wireless communication*. Cambridge university press, 2005.
- [9] L. Dai, B. Wang, Y. Yuan, S. Han, I. Chih-Lin, and Z. Wang, "Non-orthogonal multiple access for 5G: solutions, challenges, opportunities, and future research trends," *IEEE Communica*tions Magazine, vol. 53, no. 9, pp. 74–81, Sept. 2015.
- [10] H. Vikalo and B. Hassibi, "The expected complexity of sphere decoding, part I: Theory, part II: Applications," *IEEE Transac*tions on Signal Processing, vol. 53, no. 8, p. 2819–2834, Aug. 2003.
- [11] A. Wiesel, Y. C. Eldar, and S. Shamai, "Semidefinite relaxation for detection of 16-QAM signaling in MIMO channels," *IEEE Signal Processing Letters*, vol. 12, no. 9, pp. 653–656, Aug. 2005

- [12] U. Madhow and M. L. Honig, "MMSE interference suppression for direct-sequence spread-spectrum CDMA," *IEEE Transactions on Communications*, vol. 42, no. 12, pp. 3178–3188, Dec. 1994.
- [13] E. Björnson, J. Hoydis, and L. Sanguinetti, "Massive MIMO networks: Spectral, energy, and hardware efficiency," *Founda*tions and *Trends in Signal Processing*, vol. 11, no. 3-4, pp. 154–655, 2017.
- [14] O. Elijah, C. Y. Leow, T. A. Rahman, S. Nunoo, and S. Z. Iliya, "A comprehensive survey of pilot contamination in massive MIMO—5G system," *IEEE Communications Surveys & Tutorials*, vol. 18, no. 2, pp. 905–923, Aug. 2015.
- [15] H. Hotelling, "Relations between two sets of variates," *Biometrika*, vol. 28, no. 3/4, pp. 321–377, 1936.
- [16] D. R. Hardoon, S. Szedmak, and J. Shawe-Taylor, "Canonical correlation analysis: An overview with application to learning methods," *Neural Computation*, vol. 16, no. 12, pp. 2639–2664, 2004.
- [17] M. S. Ibrahim and N. D. Sidiropoulos, "Reliable detection of unknown cell-edge users via canonical correlation analysis," *IEEE Transactions on Wireless Communications*, vol. 19, no. 6, pp. 4170–4182, Mar. 2020.
- [18] A. Dogandzic and A. Nehorai, "Finite-length MIMO equalization using canonical correlation analysis," *IEEE Trans. on Sig. Process.*, vol. 50, no. 4, pp. 984–989, Aug. 2002.
- [19] Z. Bai, G. Huang, and L. Yang, "A radar anti-jamming technology based on canonical correlation analysis," in *International Conference on Neural Networks and Brain*, vol. 1, China, Oct. 2005, pp. 9–12.
- [20] M. S. Îbrahim and N. D. Sidiropoulos, "Weak target detection in MIMO radar via beamspace canonical correlation," in *IEEE 11th Sensor Array and Multichannel Signal Processing Workshop* (SAM), Hangzhou, China, June 2020, pp. 1–5.
- [21] A. Bertrand and M. Moonen, "Distributed canonical correlation analysis in wireless sensor networks with application to distributed blind source separation," *IEEE Trans. on Sig. Process.*, vol. 63, no. 18, pp. 4800–4813, 2015.
- [22] M. Borga and H. Knutsson, "A canonical correlation approach to blind source separation," Report LiU-IMT-EX-0062 Department of Biomedical Engineering, Linkping University, 2001.
- [23] M. S. Ibrahim, A. S. Zamzam, A. Konar, and N. D. Sidiropoulos, "Cell-edge detection via selective cooperation and generalized canonical correlation," *IEEE Trans. on Wir. Commun.*, vol. 20, no. 11, pp. 7431–7444, June 2021.
- [24] R. Arora and K. Livescu, "Multi-view learning with supervision for transformed bottleneck features," in *IEEE International Con*ference on Acoustics, Speech and Signal Processing (ICASSP), Italy, May 2014, pp. 2499–2503.
- [25] C. I. Kanatsoulis, X. Fu, N. D. Sidiropoulos, and M. Hong, "Structured sumcor multiview canonical correlation analysis for large-scale data," *IEEE Trans. on Sig. Process.*, vol. 67, no. 2, pp. 306–319, Jan 2019.
- [26] J. D. Carroll, "Generalization of canonical correlation analysis to three or more sets of variables," in *Proceedings of the 76th* annual convention of the American Psychological Association, vol. 3, 1968, pp. 227–228.
- vol. 3, 1968, pp. 227–228.
  [27] A. Paulraj and C. Papadias, "Space-time processing for wireless communications," *IEEE Signal Processing Magazine*, vol. 14, no. 6, pp. 49–83, Nov. 1997.
- [28] M. S. Ibrahim and N. Sidiropoulos, "Cell-edge interferometry: Reliable detection of unknown cell-edge users via canonical correlation analysis," in *IEEE Int. Conf. on Sig. Proc. Adv. in Wir. Comm. (SPAWC)*, France, Jul. 2019, pp. 1–5.
- [29] C. Shepard, H. Yu, N. Anand, E. Li, T. Marzetta, R. Yang, and L. Zhong, "Argos: Practical many-antenna base stations," in *Proceedings of the 18th annual international conference on Mobile computing and networking*, Istanbul, Turkey, Aug. 2012, pp. 53–64.



Mohamed Salah Ibrahim (Member, IEEE) received the B.Sc. degree (Hons.) in electrical engineering from Alexandria University, Alexandria, Egypt, in 2013, the M.Sc. degree in wireless technologies from Nile University, Giza, Egypt, in 2016, and the Ph.D. degree in electrical engineering from the University of Virginia, Charlottesville, VA, USA, in 2021. He is currently a senior engineer in the Research and Innovation Department in InterDigital Communications, Conshohocken, PA, USA. His research interests include wireless communications.

signal processing, optimization, and machine learning. He was a finalist of the Best Student Paper Competition at IEEE SPAWC 2018. He has held R&D internships with FutureWei Technologies (Huawei), Chicago, IL, and Nokia Bell Labs, Murray Hill, NJ. He has received the Louis T. Rader Graduate Research Award from the University of Virginia in 2021.



Ahmed Hussain is an undergraduate working towards a B.S. in Computer Engineering and Physics at the University of Virginia in Charlottesville, Virginia with an expected graduation of May 2023. He is an REU student in Prof. Sidiropoulos' lab, working on wireless communications and software-defined radio. Ahmed is also the Electrical Director for the UVA Solar Car Team, an Electronic Controls intern at QC82 (a photonic quantum computing startup based in Maryland), and a former Embedded Systems Intern for the Battery Management Systems

team at Tesla Motors during summer 2022. His research interests lie in signal processing, robotics, and machine learning, with a particular interest in quantum computing.



Nicholas D. Sidiropoulos (Fellow, IEEE) received the Diploma in electrical engineering from the Aristotle University of Thessaloniki, Thessaloniki, Greece, and the M.S. and Ph.D. degrees in electrical engineering from the University of Maryland at College Park, College Park, MD, USA, in 1988, 1990, and 1992, respectively. He is the Louis T. Rader Professor at the University of Virginia. He has previously served on the faculty of the University of Minnesota, and the Technical University of Crete, Greece. His research interests are in signal

processing, communications, optimization, tensor decomposition, and factor analysis, with applications in machine learning and communications. He received the NSF/CAREER award in 1998, and the IEEE Signal Processing Society (SPS) Best Paper Award in 2001, 2007, and 2011. He served as IEEE SPS Distinguished Lecturer (2008–2009), as Vice President - Membership of IEEE SPS (2017–2019), and as chair of the SPS IEEE Fellow Evaluation Committee (2020-2021). He received the IEEE Signal Processing Society Meritorious Service Award (2010), the Distinguished Alumni Award of the Department of ECE, University of Maryland (2013), and the EURASIP Technical Achievement Award (2022). He is a Fellow of EURASIP (2014).